Ab initio study of the dielectric response of crystalline ropes of metallic single-walled carbon nanotubes: Tube-diameter and helicity effects

A. G. Marinopoulos,[1] Lucia Reining,[2,3] and Angel Rubio[3,4]
[1]*Department of Physics, CEMDRX, University of Coimbra, P-3004-516 Coimbra, Portugal*
[2]*Laboratoire des Solides Irradiés, Ecole Polytechnique, CNRS-CEA/DSM, 91128 Palaiseau Cedex, France*
[3]*European Theoretical Spectroscopy Facility (ETSF)*
[4]*Departamento de Física de Materiales, Facultad de Químicas, Centro Mixto CSIC-UPV/EHU, Universidad del País Vasco, 20018 San Sebastián/Donostia, Spain and Donostia International Physics Center (DIPC), 20018 San Sebastián/Donostia, Spain*
(Received 25 March 2008; revised manuscript received 7 November 2008; published 19 December 2008)

The dielectric-response functions of crystalline ropes of metallic single-walled carbon nanotubes were determined from time-dependent density-functional theory in the random-phase approximation. Interband transitions and plasmonic excitations were studied as a function of momentum transfer. The impact of the tube diameter was shown for the (n,n) armchair-type series (n ranging from 3 to 8) covering a diameter range from 4 to 11 Å. Helicity effects were examined for the thinnest tubes, the armchair (3,3) versus the zigzag (5,0) configurations. Our results give detailed insight into the various kinds of excitations that can be observed in ropes of nanotubes. Recent experimental findings and trends by electron energy loss and Raman spectroscopies are reproduced and explained.

DOI: 10.1103/PhysRevB.78.235428 PACS number(s): 71.45.−d, 78.67.−n, 79.20.Uv, 81.07.De

I. INTRODUCTION

Carbon nanotubes represent a unique phase of carbon composed of cylindrically rolled graphene sheets of various diameters and helicities. They possess a number of intriguing properties owing to their quasi-one-dimensional structure and their chemical bonding. Their electronic structure and excitations have been under intense investigation by both theoretical and experimental means.[1–4] The characteristic low-lying singularities in the density of states were determined for tubes of various diameters and helicities. The earliest theoretical predictions suggested that under certain conditions (neglect of curvature and $\pi-\sigma$ hybridization), the electronic structure of single-walled nanotubes could be interpreted in terms of the two-dimensional band structure of the graphene sheet.[5] Electron spectroscopies[6,7] are powerful experimental tools which can probe the internal electronic structure of the tubes. In particular, electron energy-loss spectroscopy (EELS) has been recently employed to analyze the dielectric response of isolated carbon nanotubes[2,8] as well as of bulk polycrystalline samples of nanotubes.[9–12]

By theoretical means, the existing research on the dielectric response of carbon nanotubes falls under three categories: (a) Model calculations[13] based on an electron-gas treatment of the response; (b) tight-binding calculations[14] based on a π-electron Hamiltonian. These calculations were done for a large variety of chiral and nonchiral nanotubes of various diameters and helped to elucidate aspects of the response in a frequency range up to 15 eV, where $\pi\rightarrow\pi^{\star}$ excitations dominate. (c) First-principles calculations based on either many-body perturbation theory[15–17] or density-functional[18–22] and Hartree-Fock[23,24] time-dependent frameworks using different approximations for exchange-correlation effects. Unfortunately, such calculations are still restricted to nanotubes of very small diameters (around 4 Å in most cases) and to the lower part of the valence-electron excitation spectrum.[17] This makes the direct comparison to most existing experiments very problematic, especially to the EELS experiments that probe the plasmonic excitations.[10–12]

The aim of the present study has been to extend the first-principles calculations of the dielectric response to carbon nanotubes of larger diameters and higher energies allowing, therefore, more rigorous comparisons with the existing experimental studies of electronic excitations of metallic nanotubes; in particular, momentum-dependent EELS data for crystalline ropes of single-walled nanotubes with very narrow distributions of mean-nanotube diameters[10–12] and Raman data on individual (isolated) nanotubes of well characterized diameters and helicities.[4]

The dielectric and electron energy-loss functions of crystalline ropes of carbon nanotubes were calculated *ab initio* for a range of magnitudes of momentum transfer q for which the energy-loss function was accessed experimentally by EELS. The calculations were based on the random-phase approximation (RPA) with inclusion of the crystal local-field effects (LFEs) in the response for the cases that this is necessary. This approximation was found sufficient in an earlier study of the optical absorption of small-diameter carbon tubes[19] predicting absorption-peak positions in very good agreement with experiment[25] and more elaborate calculations[15] that considered excitonic effects. Furthermore, our EELS calculations in graphite matched very well the experimentally observed spectra and plasmon-peak positions.[26,27] Here, we focus on the armchair series of carbon tubes, namely, of the type (n,n) with the index n ranging from 3 to 8, covering a diameter range up to roughly 11 Å. This allowed us to study systematically the induced changes in the dielectric functions with increasing tube diameter for these metallic tubes.[28] The impact of different helicities on the response of metallic tubes was also examined by comparing the results for the armchair (3,3) and zigzag (5,0) tubes, which have very similar diameters (close to 4 Å). Recent theoretical calculations of the optical-absorption spectra for these tubes showed that the position of the ab-

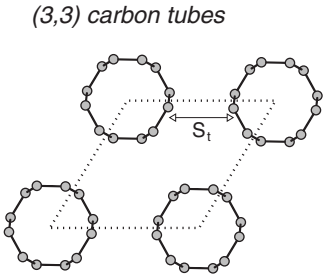

FIG. 1. Hexagonal unit cell for the (3,3) carbon tubes. S_t denotes the interwall separation.

sorption peaks is very sensitive to tube helicity.[15,18,19] In contrast, the energy-loss function in the range of the $\pi+\sigma$ plasmon and in the vanishing-q limit did not exhibit a helicity dependence.[19,20] Here, however, we provide a more complete assessment of the effect of different helicities by making the comparisons in an extended range of q. This represents a more realistic situation since the experimental EELS data are always obtained for finite momentum transfer q. Furthermore, a large value of q represents shorter wavelength perturbation and, therefore, different tubular helicities may lead to different response.

II. THEORETICAL FRAMEWORK

To model crystalline ropes of nanotubes we constructed unit cells with three-dimensional periodic boundary conditions where the infinite-length single-walled nanotubes are perfectly aligned and arranged in a hexagonal lattice (see Fig. 1). This is consistent with the experimental observations[10,29] where the obtained Bragg spectra also infer a hexagonal lattice for the nanotubes (of the order of 100–500) that make up the ropes. Nonetheless, generally bulk nanotube samples comprise finite-length nanotubes of various helicities. At present, it is not computationally feasible to model either nanotubes of long finite sizes (of the order of micrometer) or variable helicities within a single unit cell, much less to calculate their dielectric response from first principles. However, recent tight-binding calculations[30] of optical properties showed that the spectra of sufficiently long tubes (at least micrometer long) are almost the same with those of infinite-long ones. Therefore, at least for long nanotubes the present approach is justified. Edge effects originating from the finite size of short nanotubes are beyond the scope of the present work. Such effects were shown to determine the antenna properties of nanotubes in the microwave range.[31]

The present approach also neglects finite-size effects that may arise due to the finite lateral size of the ropes (number of individual tubes within a rope). This is necessitated by computational simplicity that motivates our choice of periodic boundary conditions. It is justified by the fact that the wavelengths of the perturbations considered in this momentum-resolved EELS study (range from around 100 Å down to the level of interatomic distances) are smaller than typical rope diameters. For instance, 500 tubes of the (8,8) type would yield a rope diameter approximately of 350 Å. Hence, it is the specific diameter and internal structure and properties of individual tubes and their coupling within the ropes that is the governing factor to the dielectric response. Moreover, we concentrate on perturbations parallel to the tubes axes. Finite-size effects in the lateral dimension are important for longer wavelengths; this has been illustrated in a recent study of guided-wave propagation in an isolated rope of N metallic nanotubes.[32] In that work, the geometric resonances of the electromagnetic waves were determined in the terahertz and midinfrared ranges. These modes displayed a frequency dependence that varied according to the lateral size of the rope (number of tubes).

The ground state[33] of the carbon nanotubes was determined within density-functional theory (DFT) in the local-density approximation.[34] For the valence-core interaction we used norm-conserving pseudopotentials generated from free-atom calculations.[35] The crystalline valence-electron wave functions were expanded using a plane-wave basis set and an energy cutoff of 44 Ry.

The structural relaxation consisted of minimizing the total internal energy of the unit cell with respect to total-volume changes and to atomic positions. The optimization for all the tubes studied in this work yielded interwall distances within a narrow range from 3.0 to 3.2 Å, namely, somewhat smaller than the intersheet spacing in graphite (~3.4 Å). This is also in agreement with earlier DFT calculations[36] of crystalline packings of the (6,6) carbon tubes where the hexagonal close-packed configuration was found to have the lowest energy.

The effect of different mutual rotations between neighboring tubes was studied for selected cases only and it was not found important in the dielectric-response functions, in agreement with earlier calculations of the optical absorption of (3,3) carbon tubes as a function of rotation.[22]

From the resulting Kohn-Sham eigenvalues and wave functions the linear-response independent-particle polarizability χ_0 was constructed.[37] Within time-dependent density-functional theory (TDDFT),[38] the full polarizability χ is obtained from χ_0 via the Dyson-type expression[39]

$$\chi = \chi_0 + \chi_0(V_c + f_{\mathrm{xc}})\chi, \tag{1}$$

where V_c is the bare Coulomb interaction and f_{xc}, the so-called exchange-correlation (xc) kernel, is the functional derivative of the xc potential with respect to the electron density. By setting f_{xc} to zero, xc effects in the electron response are neglected and one obtains the random-phase approximation (RPA). This approximation is justified when xc effects are small or when they cancel to a large extent: indeed, the kernel f_{xc} simulates, with respect to DFT-RPA, both a gap opening and the lowering of excitation energies due to electron-hole attraction, hence two effects of opposite sign. This explains the success of the RPA in many cases, including the description of nanotubes. Since we are moreover mostly interested in pointing out tendencies in the present work, we can safely adopt the RPA in the following.

The inverse longitudinal microscopic dielectric function[37,40] for a periodic system is obtained as

$$\varepsilon^{-1}_{\mathbf{G},\mathbf{G}'}(\mathbf{q}) = \delta_{\mathbf{G},\mathbf{G}'} + V_c(\mathbf{q}+\mathbf{G})\chi_{\mathbf{G},\mathbf{G}'}(\mathbf{q}), \quad (2)$$

with $\mathbf{q}$ in the first Brillouin zone and $\mathbf{G},\mathbf{G}'$ are reciprocal-lattice vectors. The electron energy-loss function for a transferred momentum $(\mathbf{q}+\mathbf{G})$ is given by $-\mathrm{Im}[\varepsilon^{-1}_{\mathbf{G},\mathbf{G}}(\mathbf{q})] = -\mathrm{Im}[V_c(\mathbf{q}+\mathbf{G})\chi_{\mathbf{G},\mathbf{G}}(\mathbf{q})]$. In general, due to the inhomogeneity in the electron response, $\varepsilon_{\mathbf{G},\mathbf{G}'}$ cannot be considered as being purely a diagonal matrix in the $\mathbf{G}$ space and LFE need to be accounted for: the off-diagonal elements of $\varepsilon_{\mathbf{G},\mathbf{G}'}$ have to be included in the matrix inversion. Making the approximation $\varepsilon^{-1}_{\mathbf{G},\mathbf{G}}(\mathbf{q}) \approx 1/\varepsilon_{\mathbf{G},\mathbf{G}}(\mathbf{q})$ corresponds to neglecting the inhomogeneity of the response, i.e., to neglecting the LFE.

In the sections that follow we shall present our results[41] on the q-dependent macroscopic dielectric function ε_M which is defined as $\varepsilon_M(\mathbf{q}) = 1/\varepsilon^{-1}_{\mathbf{0},\mathbf{0}}(\mathbf{q})$. The imaginary part of this function, in the vanishing q limit, gives the optical absorption. For the specific case where LFE are neglected, $\varepsilon_M(\mathbf{q}) = \varepsilon_{\mathbf{0},\mathbf{0}}(\mathbf{q})$. Accordingly, the energy-loss function is obtained as $-\mathrm{Im}(1/\varepsilon_M)$. The direction of $\mathbf{q}$ is always along the tube axis. For this polarization, it was shown[19] that the peak positions in the optical-absorption spectra are not affected by the intertube interaction, allowing therefore comparison of the present results with Raman experiments[4] on isolated nanotubes. It is also important to note here that for more general $\mathbf{q}$ orientations, the dielectric response will be modified; recent calculations[20] of the EELS spectra for the (3,3) tubes showed that for $\mathbf{q}$ components perpendicular to the tubes axis the spectra became more diffuse with increasingly more important LFE that leads to a shift of the plasmon peaks to higher frequencies. This is to be expected to a certain degree in realistic situations owing to the orientational disorder in bulk samples where the individual tubes in the ropes are not perfectly aligned.

The frequency range studied covers the valence-electron excitations in the form of interband and intraband (for finite q) transitions and plasmonic excitations up to 45 eV for some cases. Very low frequencies in the terahertz range are extremely difficult to treat with the TDDFT framework adopted here and are beyond the scope of the present work. For the same reason, tunneling of free carriers between atoms on different tubes is also neglected. Tunneling effects for a rope of metallic tubes were calculated using a nearest-neighbor tight-binding Hamiltonian in Ref. 42. As expected, these effects were confined at very low energies (to within 0.1 eV of the Fermi energy) and were responsible for the creation of a pseudogap in the density of states at the Fermi energy.

III. q-DEPENDENT RESPONSE AND DIAMETER DEPENDENCE

In this section the calculated q-dependent dielectric functions are reported for crystalline ropes of armchair-type tubes as a function of tube diameter.

For small $q = 0.23$ Å^{-1}, the imaginary part of ε_M and energy-loss functions for several armchair tubes are plotted in Fig. 2. It can be seen that for all tubes $\mathrm{Im}[\varepsilon_M(\mathbf{q})]$ exhibits an intense structure in the 0–5 eV frequency range due to $\pi \rightarrow \pi^\star$ electron excitations. The shape of this structure be-

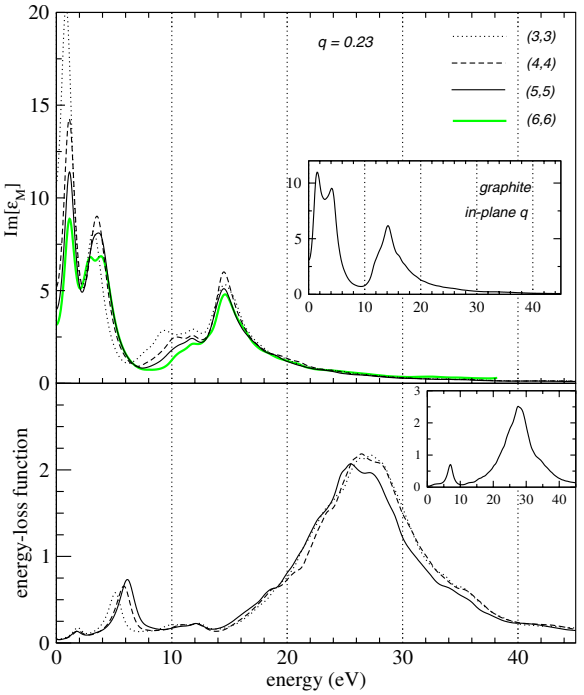

FIG. 2. (Color online) Dielectric (imaginary part) and energy-loss function for the (3,3), (4,4), and (5,5) tubes calculated for a small (0.23 Å^{-1}) momentum-transfer $\mathbf{q}_\parallel$ parallel to the tubes axis. The $\mathrm{Im}[\varepsilon_M]$ is also plotted for the (6,6) tubes. The results were obtained without LFE. The insets contain the corresponding results for graphite (from Ref. 26). Broadening is set to 0.5 eV.

comes broader and more uniform with increasing tube diameter. The calculated spectrum for the (6,6) tubes resembles the graphitic one for in-plane polarization (displayed in the upper inset in Fig. 2). In the 8–12 eV range a shoulderlike feature develops which is especially evident for the smaller-diameter (3,3) and (4,4) tubes; it is very much attenuated for the larger-diameter (5,5) and (6,6) ones and absent in the graphitic absorption spectrum. This suggests that the origin of this feature is the strong tubular curvature which promotes $\pi-\sigma$ hybridization. At higher frequencies, beyond 12 eV, a more intense structure is seen with a prominent peak at 14.5 eV. This structure reflects the contribution of $\sigma \rightarrow \sigma^\star$ interband transitions and it is also observed in the absorption spectrum of graphite for in-plane $\mathbf{q}$ (Refs. 26 and 27) (see inset) with very similar shape and peak position.

The corresponding energy-loss function contains three distinct plasmon peaks (see lower panel in Fig. 2): first, the intraband plasmon in the 1–2 eV range. This plasmon arises from the collective oscillations of the free carriers of the linear bands which cross at/near the Fermi energy.[43] This crossing is a common characteristic of all armchair-type tubes[1,2] and it is, therefore, a fingerprint of metallicity irrespective of the index n. At higher frequencies, the two valence-electron plasmons are found in the 5–7 eV range (π plasmon) and in the 26–28 eV range (the total $\pi+\sigma$ plasmon).[44] In agreement with experimental energy-loss data obtained from bulk single-walled nanotube material[10] we find hence the two valence plasmons to be consistently lower in energy than in graphite (see inset) where the plas-

mon energies for small in-plane q are 7.2 and 28 eV, respectively.[27]

The higher-energy $\pi+\sigma$ plasmon peak does not display a strong diameter dependence. For the (5,5) case it is slightly displaced to a lower frequency; this is consistent with the average electron density being smaller for this larger-diameter tube, therefore, lowering the plasmon frequency according to homogeneous electron-gas theory.[45] It is noteworthy that the experimentally measured[10] frequency of the $\pi+\sigma$ plasmon (for the same magnitude of q) is almost 23.5 eV, namely, even lower than the present results. Given the fact that the reported mean diameter of the tubes contained in the bulk samples used in those experiments was 14 Å, such a redshift of the plasmon frequency is consistent with our explanation. The redshift may also be understood as an effect of the weakening of the *intratube* interaction. The diametrically opposed wall segments will interact more weakly at larger distances with increasing tube diameter, yielding a downward shift of the plasmon frequency. A similar effect was observed in our previous study[27] of the dielectric response in graphite and in graphene-sheet geometries of various intersheet distances: smaller intersheet distances lead to $\pi+\sigma$-plasmon peaks at higher frequencies.

The two low-energy plasmons, on the other hand, exhibit more noticeable changes with increasing tube diameter and were studied in more detail. Their dispersion (q-dependent energies) was also obtained through the q-dependent energy-loss function. This function was calculated in the frequency range up to 10 eV without considering LFE in the response. This assumption was found to be valid for the range of tube diameters and q's studied (up to 0.6 $Å^{-1}$) and for **q** orientations parallel to the tubes axes.[46] Calculations including LFE (to be presented in Sec. IV) for the small-diameter tubes confirm the validity of our assumption: LFEs start to develop only after 20 eV under these conditions. The detailed energy-loss function is plotted in Fig. 3 for the (3,3), (5,5), and (7,7) tubes. The dispersion of the π plasmon is plotted in Fig. 4 for all the tubes studied in the present work where it can be seen how it disperses toward higher energies with increasing q. The experimentally observed[10] q-dependent energies of the π plasmon in bulk samples of carbon nanotubes are in the same range, albeit with a stronger dispersion (compared to the predicted dispersion for either of the tubes studied here): they are confined[10] within the 5–7.5 eV range for q's up to 0.6 $Å^{-1}$. The fact that the samples used contained a mixture of nonperfectly aligned tubes of a mean tube diameter equal to 14 Å may explain the larger scatter of the π-plasmon energies in the experimental EELS data.

These results (see Fig. 3) clearly show that the π plasmon is a well-defined peak in the energy-loss function and persists even up to 0.6 $Å^{-1}$. The intraband plasmon, however, exhibits a considerable decay [especially for the larger-diameter (7,7) tubes] and seizes to exist for the large q values considered here, e.g., 0.41 $Å^{-1}$ and beyond. The two lower-energy plasmons also display a contrasting behavior as a function of increasing tube diameter. The π-plasmon peaks (in contrast to the intraband plasmon) are progressively displaced to higher frequencies with increasing tube diameter. This blueshift, however, is a highly nonlinear function of diameter: e.g., for q equal to 0.29 $Å^{-1}$, the π-plasmon frequency is 5.2 eV for the (3,3) tubes, 5.9 eV for the (4,4) ones, and then reaches a convergence for the larger-diameter tubes [almost coincident peaks at 6.6 eV for the (7,7) and (8,8) tubes] (see Fig. 4). This convergence in the plasmon frequency with increasing tube diameter is more evident for the smaller q's studied here and can provide an explanation for the fact that the measured plasmon energies in the experiments[10] (where the samples had a 14 Å mean tube diameter, namely, larger tubes to those studied here) also did not exceed 7.5 eV for a maximum momentum transfer q of 0.6 $Å^{-1}$. As a result, the graphitic π-plasmon frequency[27] (approximately 7.2 eV for 0.25 $Å^{-1}$ and 8 eV for q equal to 0.6 $Å^{-1}$) remains an upper bound for these small- and medium-diameter metallic tubes.

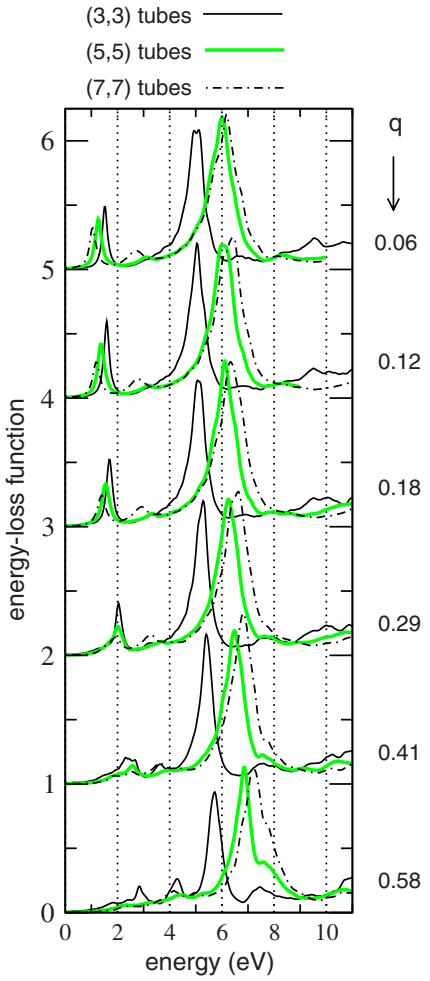

FIG. 3. (Color online) q-dependent energy-loss function for the (3,3), (5,5), and (7,7) tubes calculated for **q**-orientation parallel to the tubes axis. q is given in units of $Å^{-1}$. The results were obtained without LFE. Broadening is set to 0.1 eV.

The above behavior of the π-plasmon energy is unexpected within the context of homogeneous electron-gas theory where lower average electron densities (larger tube diameters) would be expected to yield lower plasmon energies.[45] Instead, the present results for the π plasmon suggest that the specific electronic structure of the tubes and the ensuing interband transitions must have an impact. In order to elucidate this point further, we plot in Fig. 5 the imaginary

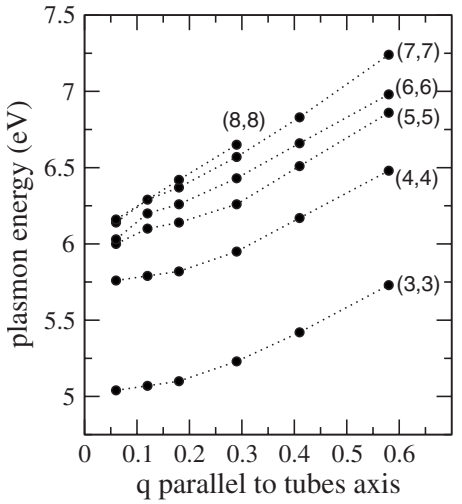

FIG. 4. Dispersion of the π plasmon for **q**-orientation parallel to the tubes axis. The momentum-transfer **q** has units of Å^{-1}. The dotted lines are guides for the eyes.

and real parts of the dielectric function versus frequency for all the tubes studied taking the smallest q of 0.06 Å^{-1}, where the imaginary part should be essentially proportional to the optical-absorption spectrum. For all the tubes very intense absorption structure is observed at energies below 1 eV. This intense oscillator strength is a consequence of the metallicity of these armchair tubes: it originates from the intraband transitions involving the two linear bands which intersect at/near the Fermi energy. At higher frequencies, the absorption is dominated by interband transitions. The major feature is an absorption band in the range from 2 to 6 eV, with a width and shape depending strongly upon tube diameter. The smallest-diameter (3,3) tubes exhibit a single absorption peak at 2.8 eV in this frequency range. The (4,4) tubes exhibit a similar spectrum, albeit wider and with the main peak at 3 eV. For the larger-diameter tubes [(5,5) and larger ones] the interband excitation spectrum is more extended and broader having a two-peak structure. The width of the absorption band and the degree of its bimodal shape progressively increase with increasing tube diameter. As a result, there is a progressive shift of the first absorption peak toward lower frequencies for the larger-diameter tubes. This behavior is in agreement with recent experimental data from resonant Raman spectroscopy[4] where interband-transition peaks of the same metallic armchair tubes were determined.

At higher frequencies, starting at 8 eV, the smaller-diameter tubes [especially the (3,3) ones] exhibit an absorption structure which is nonexistent in graphite[27] and which progressively diminishes in intensity with increasing tube diameter (see Fig. 5; also discussed in Fig. 2 for slightly larger q). These transitions in this frequency range (caused by the increased $\pi-\sigma$ hybridization in the smaller-diameter tubes) lead to an increase of the macroscopic screening: the real part of the dielectric function (which is negative in this range) increases more abruptly and eventually takes positive values at lower frequencies for the lower-diameter tubes (see Fig. 5). Consequently, the zero of Re$[\varepsilon_M(\mathbf{q})]$ (i.e., vanishing magnitude of the real part of the longitudinal dielectric function; the plasmon-existence criterion) takes place at lower frequencies. This explains the progressive shift of the π-plasmon position as a function of diameter. In contrast, the behavior of the intraband plasmon (see Fig. 3) can be understood as follows. The broadening of the interband-absorption spectrum and the redshift of the first (interband) absorption peak for the larger-diameter tubes (see Fig. 5) causes a progressive shift of the zero of Re$[\varepsilon_M(\mathbf{q})]$ (zero positions denoted by the arrows in Fig. 5) and, consequently, of the intraband plasmon peak toward lower frequencies. It is interesting to note that the experimental energy-loss data[12] in this frequency range also exhibited the same characteristics in terms of the peak positions for samples of different mean tube diameters. Namely, the observed peaks in the 0.5–2.0 eV range were found at lower frequencies for the samples with the larger mean tube diameters. Although the measured samples contained tubes of different chiralities and orientations, the above agreement leads us to suggest that the origin of the observed low-frequency peaks in the experimental loss

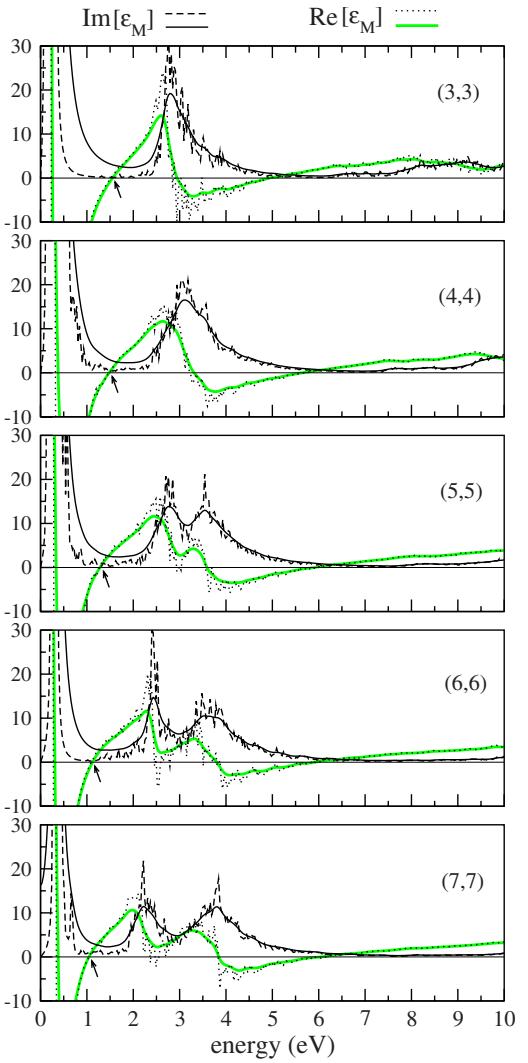

FIG. 5. (Color online) Dielectric function of the tubes in the 0–10 eV range for small q (equal to 0.06 Å^{-1}) of orientation parallel to the tubes axis. Results obtained without LFE. Full curves denote corresponding results with a broadening of 0.1 eV.

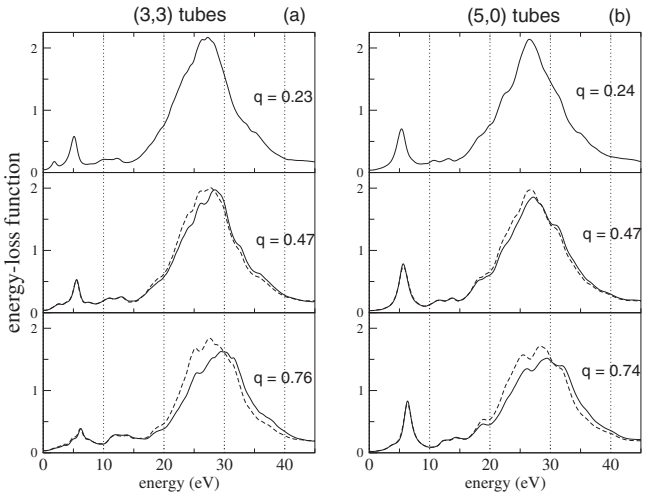

FIG. 6. q-dependent energy-loss function of the (3,3) and (5,0) tubes. $\mathbf{q}$ is parallel to the tube axis. Solid (dashed) curves denote results obtained with (without) LFE. Broadening is set to 0.5 eV.

data must be the intraband plasmons of the metallic armchair-type tubes which, as shown above, are influenced by both intraband and interband transitions in a quite intricate way. In order to explain the observations, one has hence definitely to go beyond the simple picture of interband transitions alone that was evoked in Ref. 12.

IV. q-DEPENDENT RESPONSE AND HELICITY: (3,3) VERSUS (5,0) TUBES

In this section we examine the impact of different helicity on the q-dependent response. We performed a comparative study for the very thin tubes: the armchair (3,3) and the zigzag (5,0) that have very similar diameters (approximately 4 Å) and are both metallic.

The q-dependent energy-loss function of these tubes is plotted in Fig. 6 for three representative q values. Only $\mathbf{q}$ orientations parallel to the tubes axes were again considered. For the smaller q, the energy-loss function for the (3,3) tubes displays the three distinct plasmon peaks [see Fig. 6(a)], which have been discussed in Sec. III. The (5,0) tubes, on the other hand, do not possess an intraband plasmon in the energy-loss function [see Fig. 6(b)]. Again, for the smaller q, the π plasmon peak appears at 5.2 eV, as in the (3,3) case. The total plasmon ($\pi+\sigma$) has a very similar energy and shape as its counterpart in the (3,3) tubes.

Inspection of the dielectric function in the 0–10 eV range can help to explain the occurrence (or not) of the peaks in the energy-loss function for these thin tubes. In Fig. 7(a) the dielectric function for the (3,3) tubes is plotted in the 0–10 eV range for a small $q=0.23$ Å^{-1} parallel to the tube axis. The frequencies where the real part of $\varepsilon_M(\mathbf{q})$ becomes zero are denoted by the arrows. For small q the imaginary part of $\mathrm{Im}[\varepsilon_M(\mathbf{q})]$ has small values at these frequencies and, therefore, the plasmon-existence criterion holds and well-defined plasmon excitations in the loss function are observed: the intraband and the π plasmon at ~2 and 5.2 eV, respectively. These energies are slightly higher than the energies where

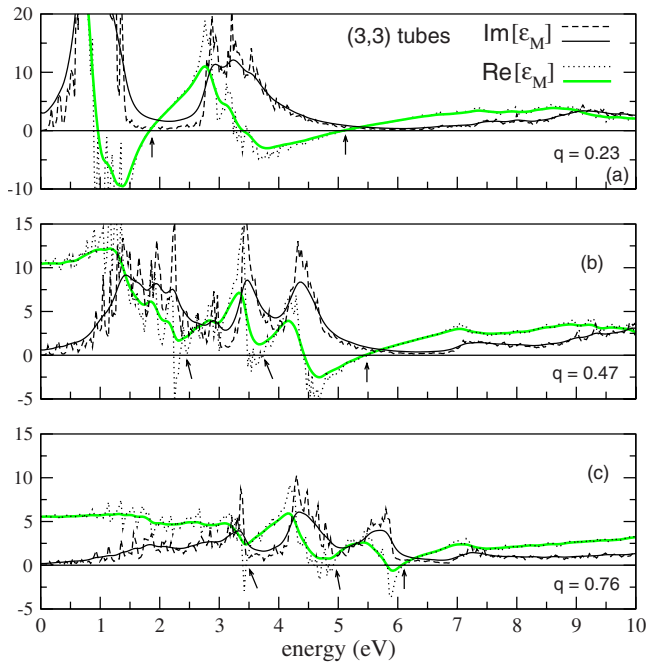

FIG. 7. (Color online) Dielectric function of the (3,3) tubes in the 0–10 eV range for three $\mathbf{q}$ vectors of orientation parallel to the tubes axis. Results obtained without LFE. Full curves denote corresponding results with a broadening of 0.1 eV.

the zeros of $\mathrm{Re}[\varepsilon_M(\mathbf{q})]$ occur (denoted by arrows), a consequence of the nonzero $\mathrm{Im}[\varepsilon_M(\mathbf{q})]$ at the zero crossing; namely, the plasmons are slightly damped from the interband transitions.

The reason for the absence of a low-energy plasmon peak in the (5,0) tubes, despite the fact that these tubes are also metallic, can similarly be traced back to the frequency dependence of the dielectric function plotted in Fig. 8(a). It can be seen from the calculated raw data that, although $\mathrm{Re}[\varepsilon_M(\mathbf{q})]$ becomes zero in the 1–2 eV range, the $\mathrm{Im}[\varepsilon_M(\mathbf{q})]$ is very large in the same frequency range attaining a magnitude equal to ~20 (assuming a 0.1 eV broadening). Therefore, the low-energy plasmon is heavily damped from the interband transitions and consequently no plasmon peak appears in the energy-loss function. This is in contrast to the situation encountered for small q for the (3,3) tube, where the zero of $\mathrm{Re}[\varepsilon_M(\mathbf{q})]$ takes place in the region of reduced absorption, between the intraband and interband absorption peaks [Fig. 7(a)].

With increasing q, the existing plasmon peaks in the energy-loss function for both types of tubes disperse toward higher energies (see Fig. 6). The only exception is the intraband plasmon in the (3,3) tubes which for larger magnitudes of q is severely damped and no longer appears as a well-defined peak. The π plasmon also reduces in intensity and becomes considerably broader. For larger q's LFEs are now more important and modify the energy-loss function for frequencies beyond 20 eV, namely, where the $\pi+\sigma$ plasmon is found. As a result, this plasmon acquires a shift of its center of gravity by as much as 2 eV [from 28 to 30 eV, for the (3,3) case] for the largest q studied here. Again even at larger magnitudes of q, the $\pi+\sigma$ plasmon remains very similar for

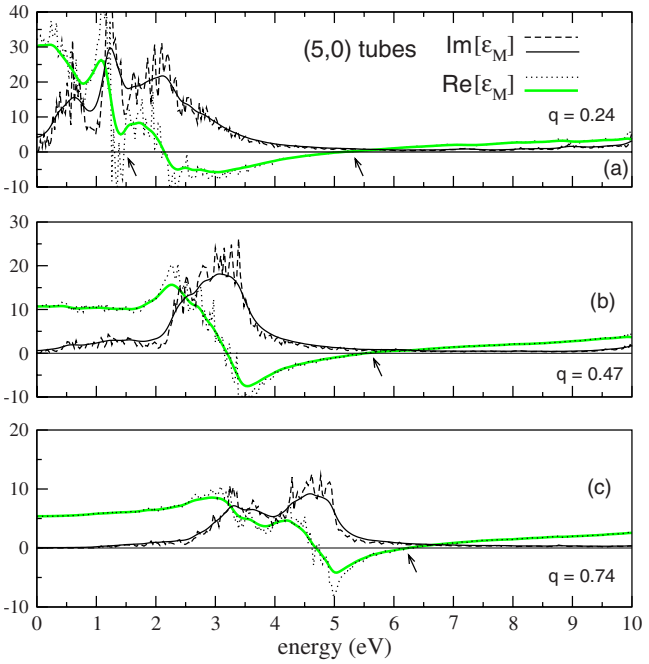

FIG. 8. (Color online) Dielectric function of the (5,0) tubes in the 0–10 eV range for three **q** vectors of orientation parallel to the tubes axis. Results obtained without LFE. Full curves denote corresponding results with a broadening of 0.1 eV.

these tubes. Its center of gravity is almost the same for both types of tubes and only a slightly larger width is observed for the (5,0) ones. It is, therefore, a helicity-independent spectroscopic quantity for a wide range of experimentally accessible q's, namely, up to 0.7 Å^{-1}.[10,11] Therefore, electron energy-loss experiments probing the $\pi+\sigma$ plasmon cannot distinguish different tube helicities even for these relatively large magnitudes of momentum-transfer q.

For finite magnitudes of q it is less certain that peaks in the energy-loss function represent well-defined plasmon-excitation modes. For sufficiently large q (shorter wavelength perturbations), individual single-particle (interband) transitions may eventually replace plasmons as the dominant excitation modes in certain frequency regions in the energy-loss function. We have checked whether the plasmon-existence criterion [vanishing of the real part of the longitudinal dielectric function $\varepsilon_M(\mathbf{q})$] also holds at larger q. For the (3,3) tubes, although Re$[\varepsilon_M(\mathbf{q})]$ has zeros in the 2–7 eV range for large q [denoted by arrows in Figs. 7(b) and 7(c)], the line shape of Im$[\varepsilon_M(\mathbf{q})]$ at the same time is more broader and couples with the plasmon excitations. This coupling yields a more diffuse line shape in the 0–10 eV range of the energy-loss function for large q. In this range only the π plasmon at approximately 6 eV may be classified as a plasmonic excitation.

In the (5,0) tubes, the situation is less complicated for larger q's. The plotted real and imaginary parts of $\varepsilon_M(\mathbf{q})$ are displayed in Fig. 8. Only one zero of Re$[\varepsilon_M(\mathbf{q})]$ is seen (its position is marked by the arrow) with very small corresponding Im$[\varepsilon_M(\mathbf{q})]$ in its neighborhood. Therefore, the π-plasmon excitation does not couple with the interband transitions and is nearly undamped. As a result, it appears as a well-defined peak in the energy-loss function of these tubes even for the larger q magnitudes (see Fig. 6).

V. CONCLUSIONS

The present calculations have provided an account of the changes in the dielectric response of crystalline ropes of metallic (armchair-type) tubes as a function of tube diameter. Although the dielectric functions of these tubes exhibited certain qualitative similarities with graphite (spectral line shapes and plasmon peak positions), nonetheless important features of the spectra were clearly intrinsic to the specific tubular dielectric response, more specifically, the existence of the low-frequency intraband plasmon in the 1–2 eV range, which is absent in graphite, as well as the development of additional spectral structure in the absorption spectrum. This structure involves a feature in the 8–12 eV range for the smaller-diameter tubes, an appearance which should be attributed to the larger tube curvatures causing increased $\sigma-\pi$ hybridization in this frequency range. It is also noteworthy that the energies of the two graphitic valence plasmons remain upper bounds for the corresponding plasmon energies in these low- and medium-diameter tubes studied here. The same finding was also observed in the existing energy-loss data from experiments[10] on polycrystalline samples of single-walled tubes of larger mean tube diameter.

In the absorption spectrum, the increase of tube diameter leads to a broader shape of the main peak structure in the 2–6 eV range. This further evolved into a two-peak absorption structure with increasing tendency of the first absorption peak to be progressively displaced to lower frequencies something which was also observed recently by Raman spectroscopy.[4] In the energy-loss spectrum the resulting changes with increasing tube diameter were studied in more detail for the intraband and π plasmons. The positions of these plasmons were found to depend on the specific dielectric response of the tubes and onset of interband transitions rather than the average electron density. We also proposed that the observed low-frequency peaks seen in the experimental energy-loss data[12] must be intraband plasmons and not interband transitions as was originally suggested. Furthermore, the calculated dispersion (q-dependent plasmon energies) showed that the π plasmon persists as a distinct excitation mode even for larger magnitudes of q and reaches a convergence in its energy with increasing tube diameter (more notably for the smaller q's). The intraband plasmon remained confined in the 1–2 eV range and was heavily damped for q's larger than 0.4 Å^{-1} and to a higher degree for the larger-diameter (7,7) and (8,8) tubes.

The impact of different helicities was only examined for the smallest-diameter (3,3) and (5,0) tubes. These tubes exhibited differences only in the low-frequency part of the energy-loss function: the (5,0) tubes (despite the fact that they are also predicted to be metallic) lacked an intraband plasmon and displayed a very intense undamped π-plasmon peak even at large momentum transfers q. The total $(\pi+\sigma)$ plasmon, on the other hand, was modified by local-field effects and did not display a helicity dependence through the range of q's considered here.

ACKNOWLEDGMENTS

This work was supported by the EC-RTN program NANOPHASE (Contract No. HPRN-CT-2000-00167), by the Spanish MEC (Contract No. FIS2007-65702-C02-01) and Grupos Consolidados UPV/EHU of the Basque Country Government (2007), and by the European Community through NoE Nanoquanta (Contract No. NMP4-CT-2004-500198), SANES (Contract No. NMP4-CT-2006-017310), DNA-NANODEVICES (Contract No. IST-2006-029192), and NANO-ERA Chemistry projects, UPV/EHU (SGIker Arina). A.R. also acknowledges support from the Ecole Polytechnique during a sabbatical leave in 2001 when this work was started. Computer time was granted by IDRIS (Project No. 544). Helpful discussions with Thomas Pichler are acknowledged.

[1] R. Saito, G. Dresselhaus, and M. S. Dresselhaus, *Physical Properties of Carbon Nanotubes* (Imperial College Press, London, 1998).

[2] See *Carbon Nanotubes: Synthesis, Structure, Properties, and Applications*, edited by M. S. Dresselhaus, G. Dresselhaus, and Ph. Avouris (Springer-Verlag, Berlin, 2001) and references therein.

[3] R. H. Baughman, A. A. Zakhidov, and W. A. de Heer, Science **297**, 787 (2002).

[4] M. S. Strano, S. K. Doorn, E. H. Haroz, C. Kittrell, R. H. Hauge, and R. E. Smalley, Nano Lett. **3**, 1091 (2003); C. Fantini, A. Jorio, M. Souza, M. S. Strano, M. S. Dresselhaus, and M. A. Pimenta, Phys. Rev. Lett. **93**, 147406 (2004); V. Barone, J. E. Peralta, and G. E. Scuseria, Nano Lett. **5**, 1830 (2005).

[5] N. Hamada, S. I. Sawada, and A. Oshiyama, Phys. Rev. Lett. **68**, 1579 (1992).

[6] H. Raether, *Excitation of Plasmons and Interband Transitions by Electrons, Springer Tracts in Modern Physics* (Springer, Berlin, 1980), Vol. 88.

[7] J. Fink, Adv. Electron. Electron Phys. **75**, 121 (1989) and references therein.

[8] R. Kuzuo, M. Terauchi, and M. Tanaka, Jpn. J. Appl. Phys., Part 2 **31**, L1484 (1992); V. P. Dravid, X. Lin, Y. Wang, X. K. Wang, A. Yee, J. B. Ketterson, and R. P. H. Chang, Science **259**, 1601 (1993); P. M. Ajayan, S. Iijima, and T. Ichihashi, Phys. Rev. B **47**, 6859 (1993); L. A. Bursill, P. A. Stadelmann, J. L. Peng, and S. Prawer, *ibid.* **49**, 2882 (1994); M. Kociak, L. Henrard, O. Stéphan, K. Suenaga, and C. Colliex, *ibid.* **61**, 13936 (2000); O. Stéphan, D. Taverna, M. Kociak, K. Suenaga, L. Henrard, and C. Colliex, *ibid.* **66**, 155422 (2002).

[9] See review article by Fink and Lambin in Ref. 2.

[10] T. Pichler, M. Knupfer, M. S. Golden, J. Fink, A. Rinzler, and R. E. Smalley, Phys. Rev. Lett. **80**, 4729 (1998).

[11] X. Liu, T. Pichler, M. Knupfer, M. S. Golden, J. Fink, D. A. Walters, M. J. Casavant, J. Schmidt, and R. E. Smalley, Synth. Met. **121**, 1183 (2001).

[12] X. Liu, T. Pichler, M. Knupfer, M. S. Golden, J. Fink, H. Kataura, and Y. Achiba, Phys. Rev. B **66**, 045411 (2002).

[13] For example, C. Yannouleas, E. N. Bogachek, and U. Landman, Phys. Rev. B **53**, 10225 (1996); F. J. García-Vidal, J. M. Pitarke, and J. B. Pendry, Phys. Rev. Lett. **78**, 4289 (1997); G. Gumbs and G. R. Aĭzin, Phys. Rev. B **65**, 195407 (2002).

[14] M. F. Lin and Kenneth W.-K. Shung, Phys. Rev. B **50**, 17744 (1994); M. F. Lin, D. S. Chuu, C. S. Huang, Y. K. Lin, and K. W.-K. Shung, *ibid.* **53**, 15493 (1996); S. Tasaki, K. Maekawa and T. Yamabe, *ibid.* **57**, 9301 (1998); M. F. Lin and D. S. Chuu, *ibid.* **57**, 10183 (1998); G. Ya. Slepyan, S. A. Maksimenko, A. Lakhtakia, O. Yevtushenko and A. V. Gusakov, *ibid.* **60**, 17136 (1999); M. F. Lin, F. L. Shyu and R. B. Chen, *ibid.* **61**, 14114 (2000); F. L. Shyu and M. F. Lin, *ibid.* **62**, 8508 (2000); A. Grüneis, R. Saito, G. G. Samsonidze, T. Kimura, M. A. Pimenta, A. Jorio, A. G. Souza Filho, G. Dresselhaus and M. S. Dresselhaus, *ibid.* **67**, 165402 (2003).

[15] C. D. Spataru, S. Ismail-Beigi, L. X. Benedict, and S. G. Louie, Phys. Rev. Lett. **92**, 077402 (2004); C. D. Spataru, S. Ismail-Beigi, L. X. Benedict, and S. G. Louie, Appl. Phys. A: Mater. Sci. Process. **78**, 1129 (2004).

[16] E. Chang, G. Bussi, A. Ruini, and E. Molinari, Phys. Rev. Lett. **92**, 196401 (2004).

[17] F. Wang, D. J. Cho, B. Kessler, J. Deslippe, P. J. Schuck, S. G. Louie, A. Zettl, T. F. Heinz, and Y. R. Shen, Phys. Rev. Lett. **99**, 227401 (2007).

[18] H. J. Liu and C. T. Chan, Phys. Rev. B **66**, 115416 (2002); M. Machón, S. Reich, C. Thomsen, D. Sánchez-Portal, and P. Ordejón, *ibid.* **66**, 155410 (2002).

[19] A. G. Marinopoulos, L. Reining, A. Rubio, and N. Vast, Phys. Rev. Lett. **91**, 046402 (2003).

[20] A. G. Marinopoulos, L. Wirtz, A. Marini, V. Olevano, A. Rubio, and L. Reining, Appl. Phys. A **78**, 1157 (2004).

[21] G. Y. Guo, K. C. Chu, D. S. Wang, and C. G. Duan, Phys. Rev. B **69**, 205416 (2004).

[22] B. K. Agrawal, S. Agrawal, R. Srivastava, and S. Singh, Phys. Rev. B **70**, 075403 (2004).

[23] H. Ajiki and T. Ando, Physica B **201**, 349 (1994); T. Ando, J. Phys. Soc. Jpn. **66**, 1066 (1997).

[24] W. Z. Liang, G. H. Chen, Z. M. Li, and Z. K. Tang, Appl. Phys. Lett. **80**, 3415 (2002).

[25] Z. M. Li, Z. K. Tang, H. J. Liu, N. Wang, C. T. Chan, R. Saito, S. Okada, G. D. Li, J. S. Chen, N. Nagasawa, and S. Tsuda, Phys. Rev. Lett. **87**, 127401 (2001); N. Wang, Z. K. Tang, G. D. Li, and J. S. Chen, Nature (London) **408**, 50 (2000).

[26] A. G. Marinopoulos, L. Reining, V. Olevano, and A. Rubio, Phys. Rev. Lett. **89**, 076402 (2002).

[27] A. G. Marinopoulos, L. Reining, A. Rubio, and V. Olevano, Phys. Rev. B **69**, 245419 (2004).

[28] Although armchair carbon tubes are intrinsically metallic, recent calculations have shown that the (3,3) and (5,0) tubes for large intertube distances display a Peierls transition towards an insulating phase at a critical temperature larger than 300 K [D. Connetable, G.-M. Rignanese, J.-C. Charlier, and X. Blase, Phys. Rev. Lett. **94**, 015503 (2005)].

[29] A. Thess, R. Lee, P. Nikolaev, H. Dai, P. Petit, J. Robert, C. Xu, Y. H. Lee, S. G. Kim, A. G. Rinzler, D. T. Colbert, G. E. Scuseria, D. Tomanek, J. E. Fischer, and R. E. Smalley, Science **273**, 483 (1996).

[30] R. B. Chen, C. P. Chang, F. L. Shyu, J. S. Hwang, and M. F. Lin, Carbon **42**, 531 (2004).
[31] G. Ya. Slepyan, M. V. Shuba, S. A. Maksimenko, and A. Lakhtakia, Phys. Rev. B **73**, 195416 (2006).
[32] M. V. Shuba, S. A. Maksimenko, and A. Lakhtakia, Phys. Rev. B **76**, 155407 (2007).
[33] The ABINIT code was employed for the ground-state calculations. This code is a common project of the Université Catholique de Louvain, Corning Incorporated, and other contributors (http://www.abinit.org).
[34] P. Hohenberg and W. Kohn, Phys. Rev. **136**, B864 (1964); W. Kohn and L. J. Sham, *ibid.* **140**, A1133 (1965); J. P. Perdew and A. Zunger, Phys. Rev. B **23**, 5048 (1981).
[35] We used the method by N. Troullier and J. L. Martins, Phys. Rev. B **43**, 1993 (1991). The pseudopotentials were generated for the $2s^2 2p^2$ atomic configuration taking a core radius of 1.46 Bohr for the wave functions.
[36] J.-C. Charlier, X. Gonze, and J.-P. Michenaud, Europhys. Lett. **29**, 43 (1995).
[37] H. Ehrenreich and M. H. Cohen, Phys. Rev. **115**, 786 (1959); S. L. Adler, *ibid.* **126**, 413 (1962); N. Wiser, *ibid.* **129**, 62 (1963).
[38] E. Runge and E. K. U. Gross, Phys. Rev. Lett. **52**, 997 (1984); E. K. U. Gross and W. Kohn, *ibid.* **55**, 2850 (1985).
[39] G. Onida, L. Reining, and A. Rubio, Rev. Mod. Phys. **74**, 601 (2002).
[40] D. Pines, *Elementary Excitations in Solids* (Benjamin, New York, 1964).
[41] When computing the polarizability matrix χ_0 in the **G** space, we used up to 22 **k** points along the tubes axis and up to 16×16 **k**-point meshes along the circumferential directions in the irreducible wedge of the Brillouin zone. We computed the matrix elements involving conduction bands up to $N=7n_{\mathrm{occ}}$, where n_{occ} is the number of occupied bands. We also considered up to 117 **G** vectors for the size of the response matrices.
[42] A. A. Maarouf, C. L. Kane, and E. J. Mele, Phys. Rev. B **61**, 11156 (2000).
[43] M. F. Lin, D. S. Chuu, and K. W.-K. Shung, Phys. Rev. B **56**, 1430 (1997).
[44] The total plasmon was only calculated for the smaller-diameter tubes (3,3), (4,4), and (5,5). For larger-diameter tubes the required summations over conduction bands in these high energies (when calculating the polarizability) needed prohibitively large computational resources.
[45] See, e.g., W. Jones and N. H. March, *Theoretical Solid State Physics* (Wiley-Interscience, New York, 1973), Vol. 1.
[46] LFE can instead become very important for larger-diameter tubes or when the system is less dense, for example, in isolated tubes [C. Kramberger, R. Hambach, C. Giorgetti, M. H. Rümmeli, M. Knupfer, J. Fink, B. Büchner, L. Reining, E. Einarsson, S. Maruyama, F. Sottile, K. Hannewald, V. Olevano, A. G. Marinopoulos, and T. Pichler, Phys. Rev. Lett. **100**, 196803 (2008)].